Damping efficiency of the Tchamwa–Wielgosz explicit dissipative scheme under instantaneous loading conditions

Laurent Mahéo, Vincent Grolleau, Gérard Rio

Damping efficiency of the Tchamwa–Wielgosz explicit dissipative scheme under instantaneous loading conditions

Laurent Mahéo [a,b,*], Vincent Grolleau [b,c], Gérard Rio [b]

[a] *Écoles militaires de Saint-Cyr Coëtquidan, laboratoire de mécanique des matériaux, 56381 Guer cedex, France*
[b] *Université de Bretagne-Sud, laboratoire d'ingénierie des matériaux de Bretagne, 56321 Lorient cedex, France*
[c] *École polytechnique, laboratoire de mécanique des solides, 91128 Palaiseau cedex, France*

Abstract

To deal with dynamic and wave propagation problems, dissipative methods are often used to reduce the effects of the spurious oscillations induced by the spatial and time discretization procedures. Among the many dissipative methods available, the Tchamwa–Wielgosz (TW) explicit scheme is particularly useful because it damps out the spurious oscillations occurring in the highest frequency domain. The theoretical study performed here shows that the TW scheme is decentered to the right, and that the damping can be attributed to a nodal displacement perturbation. The FEM study carried out using instantaneous 1-D and 3-D compression loads shows that it is useful to display the damping versus the number of time steps in order to obtain a constant damping efficiency whatever the size of element used for the regular meshing. A study on the responses obtained with irregular meshes shows that the TW scheme is only slightly sensitive to the spatial discretization procedure used.

Keywords: Dynamical systems; Structural dynamics; Explicit and dissipative time integration algorithm; Tchamwa–Wielgosz scheme

Résumé

Efficacité amortissante du schéma explicite dissipatif de Tchamwa–Wielgosz pour des chargements impulsionnels. Dans le cadre de problèmes de dynamique ou de propagation d'ondes, l'utilisation d'une méthode dissipative est souvent nécessaire pour réduire les oscillations parasites provenant des discrétisations spatiales et temporelles. Parmi les nombreuses méthodes existantes, le schéma explicite dissipatif de Tchamwa–Wielgosz amortit ces oscillations en ciblant son amortissement sur l'énergie des hautes fréquences. Une étude théorique montre ici le décentrage à droite de ce schéma et interprète son amortissement comme une perturbation des déplacements nodaux. L'étude FEM sur des cas de compression impulsionnelle 1-D et 3-D montre l'utilité d'afficher l'amortissement en fonction du nombre de pas de temps et permet d'obtenir une efficacité amortissante constante quelque soit la taille de l'élément utilisé dans le maillage régulier. L'étude de la réponse obtenue pour des maillages irréguliers montre la légère sensibilité de l'amortissement du schéma de TW à la discrétisation spatiale utilisée.

Mots-clés : Systèmes dynamiques ; Algorithme d'intégration temporelle explicite et dissipatif ; Schéma de Tchamwa–Wielgosz

* Corresponding author.
E-mail addresses: laurent.maheo@st-cyr.terre-net.defense.gouv.fr (L. Mahéo), vincent.grolleau@univ-ubs.fr (V. Grolleau), gerard.rio@univ-ubs.fr (G. Rio).

Version française abrégée

Dans le cadre de problèmes de dynamique, l'utilisation des Méthodes des Eléments Finis et des Différences Finies pour les discrétisations spatiale et temporelle fait apparaître des erreurs purement numériques. Parmi les nombreuses méthodes utilisées pour amortir ces oscillations parasites hautes fréquences, on se propose d'étudier et d'analyser l'efficacité amortissante du schéma explicite et dissipatif de Tchamwa–Wielgosz (Eqs. (1) et (4)) sous des conditions de chargements impulsionnels. La comparaison théorique avec le schéma des Différences Centrées montre le décentrage à droite de ce schéma dissipatif (Eq. (8)) pour lequel l'amortissement peut être interprêté comme une perturbation du déplacement (Eq. (6)). On montre alors la sensibilité de l'amortissement au ratio du pas de temps de calcul sur le pas de temps critique $r_{\Delta t} = \frac{\Delta t}{\Delta t_c}$. Des études 1-D et 3-D montrent ensuite la sensibilité de son amortissement à la discrétisation spatiale utilisée. En fixant les valeurs du ratio $r_{\Delta t}$ et du paramètre d'amortissement φ, on note tout d'abord l'intérêt d'exploiter les résultats de pertes d'énergie en fonction du nombre de pas de temps pour lequel l'algorithme est appliqué. On remarque alors la quasi insensibilité de l'amortissement au raffinement du maillage pourvu que les dimensions des éléments soient le plus homogène possible. Dans le cas de maillages composés d'éléments de différentes longueurs, l'efficacité amortissante diminue. Même si le chargement est impulsionnel, sa propagation à travers le maillage perd son caractère instantané puisque plusieurs pas de temps sont nécessaires pour « traverser » les plus gros éléments du maillage. En effet, pour chaque élément i, le ratio $r^i_{\Delta t} = \frac{\Delta t}{\Delta t^i_c}$ diminue ce qui provoque une perte d'efficacité amortissante. Dans le cas 3-D, la différenciation entre les propagations longitudinales faisant apparaître un ratio $r^L_{\Delta t} = \frac{\Delta t}{\Delta t^L_c}$ et transversales ($r^T_{\Delta t}$) qui sont différents confirme ces résultats.

1. Introduction

In the field of structural dynamics, the space and time discretization procedures used invariably introduce numerical errors. Damping methods are therefore often used to limit the effects of these spurious oscillations. The Bulk Viscosity method [1,2], for instance, consists in adding an artificial viscosity to the material behavior. This method has been widely used in several industrial codes such as Abaqus [3] or LS-Dyna [4]. Many implicit time integration methods can also be used for this purpose, such as the HHT [5] and WBZ [6] methods, which are based on Newmark schemes [7] and involve weighting the internal forces and the inertial forces, respectively. These two methods have been generalized by Chung and Hulbert [8]. An interesting review on this subject was published by Fung [9] in 2003. Fewer studies have dealt, however, with the use of explicit time integration methods, and the main dissipative schemes of this kind available to our knowledge are those developed by Newmark, Chung and Lee, Zhai, Hulbert and Chung, Tchamwa and Wielgosz [7,10–13].

Here it is proposed to focus on the family of algorithms involving explicit time integration schemes, especially the Tchamwa–Wielgosz (TW) scheme, because this method makes it possible to account for the high-frequency processes occurring during impact problems. Instantaneous loading conditions were adopted in order to elicit the highest possible frequencies [14] and thus to study the damping efficiency of this scheme under the most demanding frequency conditions.

Previous studies [15–18] have dealt with the damping efficiency at various TW damping parameter values and various calculation time step – to critical time step ratios. It has been established in particular that the greater this ratio is, the more efficient the damping efficiency will be. To complete this research, the influence of the meshing is studied here in the case of homogeneous and inhomogeneous 1-D and 3-D meshes. To prevent the size of calculation time step – to critical time step ratio from affecting the calculations and to obtain the same instantaneous loading conditions throughout, the same ratio was used in all the calculations.

Using viscous or plastic dissipative behavioral laws, as done by Nsiampa with the TW scheme [19], naturally results in a "filtering" process, which causes the highest frequencies in particular to disappear. To prevent the occurrence of this "natural filtering" process, which might make it difficult to assess the efficiency of the TW scheme, a linear elastic conservative law was adopted in the present study.

In Section 2, the conservative Central Differences and dissipative TW schemes are defined in the FEM context. In Section 3, the damping efficiency of the TW method is studied using a novel theoretical approach. It is established that the TW scheme is a decentered scheme and its damping is attributed to a nodal displacement perturbation. In Sections 4 and 5, various homogeneous and inhomogeneous 1-D and 3-D meshes are tested to determine the effects of the refinement and the irregularity of the meshing. The Herezh++ code developed in C++ by Rio [20] at the Laboratoire d'Ingénierie des Matériaux de Bretagne [21] was used for the FEM calculations throughout this study. In Section 6, the theoretical results and those obtained on the numerical examples studied are summarized.

2. Explicit time integration schemes

After the finite element decomposition and time discretization, the weak form of elastodynamics equilibrium leads:

$$\mathbf{M}\ddot{\mathbf{q}}_{n+1} + \mathcal{R}_{\text{int}}(\mathbf{q}_n, \mathbf{q}_{n+1}, \dot{\mathbf{q}}_n, \dot{\mathbf{q}}_{n+1}) = \mathcal{R}_{\text{ext}}(\mathbf{q}_n, \mathbf{q}_{n+1}, \dot{\mathbf{q}}_n, \dot{\mathbf{q}}_{n+1}) \tag{1}$$

where $\mathbf{M}$ is the mass matrix, $\mathcal{R}_{\text{int}}(\mathbf{q}_n, \mathbf{q}_{n+1}, \dot{\mathbf{q}}_n, \dot{\mathbf{q}}_{n+1})$ is the generalized internal force and $\mathcal{R}_{\text{ext}}(\mathbf{q}_n, \mathbf{q}_{n+1}, \dot{\mathbf{q}}_n, \dot{\mathbf{q}}_{n+1})$ is the loading force. Taking q to denote the degree of freedom for displacement, $\mathbf{q}$, $\dot{\mathbf{q}}$ and $\ddot{\mathbf{q}}$ are the nodal displacement, the velocity and the acceleration vectors, respectively. Time is discretized into time steps Δt, which are assumed here to be equal for the sake of simplicity, and the subscript n is used at time $t = n\Delta t$.

2.1. The conservative central finite difference scheme

The Central finite Difference (CD) method can be written in the form of the following equations (Géradin [22]), from which the intermediate times $n - \frac{1}{2}$ and $n + \frac{1}{2}$ have been omitted:

$$\begin{aligned} \dot{q}_{n+1} &= \dot{q}_n + \frac{\Delta t}{2}(\ddot{q}_n + \ddot{q}_{n+1}) \\ q_{n+1} &= q_n + \Delta t \dot{q}_n + \frac{(\Delta t)^2}{2}\ddot{q}_n \end{aligned} \tag{2}$$

where the velocity and the acceleration at time step n can be written:

$$\dot{q}_n = \frac{(\dot{q}_{n+\frac{1}{2}} + \dot{q}_{n-\frac{1}{2}})}{2} \quad \text{and} \quad \ddot{q}_n = \frac{(\dot{q}_{n+\frac{1}{2}} - \dot{q}_{n-\frac{1}{2}})}{\Delta t} \tag{3}$$

2.2. The dissipative Tchamwa–Wielgosz scheme

The explicit dissipative Tchamwa–Wielgosz (TW) scheme was first presented in 1997 as part of B. Tchamwa's doctoral research work [13]. This scheme is based on four parameters. The authors of subsequent consistency studies [13,15–17] have established that the algorithm can be controlled with a single parameter φ:

$$\begin{aligned} \dot{q}_{n+1} &= \dot{q}_n + \Delta t \ddot{q}_n \\ q_{n+1} &= q_n + \Delta t \dot{q}_n + \varphi(\Delta t)^2 \ddot{q}_n \end{aligned} \tag{4}$$

Stability has been studied by previous authors. For further details, see Rio et al. [17]. However, let us recall that the stability limit of this conditionally stable scheme in the undamped case ($\varphi \geqslant 1$) is $\omega\Delta t < \sqrt{\frac{2}{\varphi - \frac{1}{2}}}$ where ω is the undamped angular frequency. The evolutions of the spectral radius and the errors in the numerical damping ratio and the relative period have been studied by Nsiampa et al. [19].

3. Comparison between the CD and the TW schemes

3.1. Nodal displacement

In order to compare the displacements obtained upon applying the CD and TW schemes at a given time step, the positions q^{tw}_{n+1} given by Eq. (4) and q^{cd}_{n+1} given by Eq. (2) can be expressed in terms of q_n, $\dot{q}_n$ and $\ddot{q}_n$, i.e., in terms

of the same position, velocity and acceleration at time step n. Taking the initial position q_n and the acceleration $\ddot{q}_n$ at time step n, the two schemes differ in the velocity (Eqs. (3) and (4)). To equalize the two schemes (Eqs. (2) and (4)) at the time step prior to $(n+1)$, it suffices to make the two velocities $\dot{q}_n^{tw}$ and $\dot{q}_{n+1}^{tw}$ in the TW scheme equal to the velocities $\dot{q}_{n-\frac{1}{2}}$ and $\dot{q}_{n+\frac{1}{2}}$ in the CD scheme, which, after substituting from Eq. (3), gives:

$$\dot{q}_n^{tw} = \dot{q}_{n-\frac{1}{2}} = \dot{q}_n - \frac{\Delta t}{2}\ddot{q}_n \tag{5}$$

$$\dot{q}_{n+1}^{tw} = \dot{q}_{n+\frac{1}{2}} = \dot{q}_n + \frac{\Delta t}{2}\ddot{q}_n$$

$$q_{n+1}^{tw} = q_n + \Delta t\dot{q}_n^{tw} + \varphi(\Delta t)^2\ddot{q}_n = q_n + \Delta t\dot{q}_n + (2\varphi-1)\frac{(\Delta t)^2}{2}\ddot{q}_n = q_{n+1}^{cd} + (\varphi-1)(\Delta t)^2\ddot{q}_n \tag{6}$$

When the parameter controlling the TW scheme is equal to one, $\varphi = 1$, the displacements calculated at a given time step with the TW and CD schemes will be identical, and if the equation of equilibrium (Eq. (1)) does not depend on $\dot{q}$ and there is no viscosity, the two schemes will be equivalent.

When the parameter controlling the TW scheme is greater than one, $\varphi > 1$, the accuracy of the TW scheme will no longer be of order 2 in terms of a Taylor time development because the expression for the position q_{n+1}^{tw} will be altered by the extent of $(\varphi-1)(\Delta t)^2\ddot{q}_n$. This expression shows that the damping in the TW scheme depends on the size of the time step used to calculate Δt [17].

The displacement $(\varphi-1)(\Delta t)^2\ddot{q}$ introduces an internal force $\mathbf{K}(\varphi-1)(\Delta t)^2\ddot{q}_n$ into the equation of equilibrium, Eq. (1). In the case of a periodically oscillating displacement q, the displacement $(\varphi-1)(\Delta t)^2\ddot{q}$ will have the opposite sign to that of the displacement q_n. The TW scheme therefore yields a generalized expression for the internal force $\mathcal{R}_{\text{int}}$, which is $\mathbf{K}(\varphi-1)(\Delta t)^2\ddot{q}_n$ lower than the internal force obtained in the CD scheme, and this will lead in this case to the damping of the scheme. Note that the higher the frequency of the oscillating displacement, the greater the damping becomes.

Let us now consider an infinite 1-D mesh composed of identical linear bar elements. The natural angular frequency of the nodal displacement is given by $\omega_0 = 2\sqrt{\frac{K}{M}} = 2\frac{c}{L}\sqrt{2} = 2\frac{1}{\Delta t_c}\sqrt{2}$ where c is the sound speed, K, M, L are the rigidity, the mass and the length of the element respectively and $\Delta t_c = \frac{L}{c}$ is the critical time step of the element. At a given time step value Δt, let us introduce the calculation time step – to critical time step ratio $r_{\Delta t} = \frac{\Delta t}{\Delta t_c}$. The expression for the damping $(\Delta t)^2\ddot{q}_n$ of the natural frequency leads to: $(\Delta t)^2\ddot{q}_n = -(\Delta t)^2\omega_0^2 q_n = -(\Delta t)^2(\frac{2\sqrt{2}}{\Delta t_c})^2 q_n = -8(r_{\Delta t})^2 q_n$. Note that at a given $r_{\Delta t}$, this quantity is constant whatever the length of element adopted.

3.2. Decentered scheme

A similar expression q_{n+1}^{dv} for the position at time step $n+1$ can also be obtained by performing a second-order Taylor development on the position, taking a decentered expression for the velocity $\dot{q}_{n+\zeta}$ between time steps $(n-\frac{1}{2})$ and $(n+\frac{1}{2})$ in terms of the parameter ζ. Upon expressing $\dot{q}_{n-\frac{1}{2}}$ and $\dot{q}_{n+\frac{1}{2}}$ in terms of $\dot{q}_n$ and $\ddot{q}_n$ based on Eq. (3), we obtain:

$$\dot{q}_{n+\zeta} = (1-\zeta)\dot{q}_{n-\frac{1}{2}} + \zeta\dot{q}_{n+\frac{1}{2}} \tag{7}$$

Which gives the following equivalent relations:

$$\begin{aligned} q_{n+1}^{dv} &= q_n + \Delta t\dot{q}_{n+\zeta} + \frac{(\Delta t)^2}{2}\ddot{q}_n = q_n + \Delta t\big[(1-\zeta)\dot{q}_{n-\frac{1}{2}} + \zeta\dot{q}_{n+\frac{1}{2}}\big] + \frac{(\Delta t)^2}{2}\ddot{q}_n \\ &= q_n + \Delta t\dot{q}_{n-\frac{1}{2}} + \zeta\Delta t[\dot{q}_{n+\frac{1}{2}} - \dot{q}_{n-\frac{1}{2}}] + \frac{(\Delta t)^2}{2}\ddot{q}_n \\ &= q_n + \Delta t\dot{q}_n + \zeta(\Delta t)^2\ddot{q}_n = q_{n+1}^{cd} + \left(\zeta - \frac{1}{2}\right)(\Delta t)^2\ddot{q}_n \end{aligned} \tag{8}$$

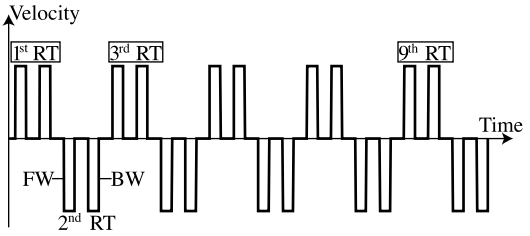

Fig. 1. Square wave propagation versus time.

The TW scheme can therefore be said to be a time integration scheme based on a decentered expression for the velocity at time step n with respect to the velocities expressed at half time steps: $\dot{q}_{n+\zeta} = (1-\zeta)\dot{q}_{n-\frac{1}{2}} + \zeta\dot{q}_{n+\frac{1}{2}}$. This gives $\varphi = \zeta + \frac{1}{2}$, and since $\varphi \geqslant 1$, $\zeta \geqslant \frac{1}{2}$ and the scheme is decentered to the right.

To obtain the corresponding damping as in previous studies [14,16,17], the value of the damping parameter φ is taken to be equal to 1.0332 throughout the following numerical study. The scheme is therefore slightly decentered to the right and Eq. (7) gives $\dot{q}_{n+\zeta} = 0.4668\dot{q}_{n-\frac{1}{2}} + 0.5332\dot{q}_{n+\frac{1}{2}}$.

4. One-dimensional damping efficiency under instantaneous loads

4.1. Description of the 1-D problem

We take the case of a cylindrical rod with a length of $L_{\text{rod}} = 200$ mm and a cross-sectional area of $S = 10\ \text{mm}^2$, which is discretized into $n_l = 100$ linear bar elements L_i in length. One end of the rod is fixed and an instantaneous compression load $P_0 = 10$ N with a square wave shape is applied to the free end:

- the pressure ramps P_0 at the beginning and $-P_0$ at the end of the square wave are simulated in $1\Delta t$,
- and the plateau duration is equal to $48\Delta t$.

The bar is assumed to be made of steel with an elastic modulus $E = 210$ GPa and a density $\rho = 8000\ \text{kg m}^{-3}$. The load applied here does not give rise to any plasticity. Linear elastic behavior is therefore adopted throughout the study. The time integration procedure implemented in the code was based on the lumped (diagonal) mass matrix. The global critical time step $\Delta t_c = \frac{L_{\min}}{c}$ is about 3.9×10^{-7} s, where $L_{\min}$ is the length of the smallest element and $c = \sqrt{\frac{E}{\rho}}$ is the sound speed in the material.

To prevent the size of time step from affecting the calculations [17], the same global ratio $r_{\Delta t} = \frac{\Delta t}{\Delta t_c} = 90\%$ was used in all the calculations. In this study, the local critical time step $\Delta t_c^i = \frac{L_i}{c}$ was defined with each element i, which gives the local ratio $r_{\Delta t}^i = \frac{\Delta t}{\Delta t_c^i}$.

4.2. Damping efficiency

The theoretical nodal velocity of the node located at the middle of the rod ($x_{\text{node}} = 100$ mm) is plotted in Fig. 1 as a function of time. Two square waves are observed for each round trip, the first is moving from the free to the fixed end (forward, FW) while the second is moving from the fixed to the free end (backward, BW). The sign of the velocity changes each time the wave is reflected from the free end.

For simplicity, the nodal velocities along the 200 mm cylindrical rod are plotted in Fig. 2 for the first, third and ninth forward waves. The 3rd and 9th waves are shifted vertically by 25 mm/s and 50 mm/s, respectively; the red line depicts the theoretical solution of the continuum problem.

In the case of the conservative CD scheme (Fig. 2(a)), the wave seems to oscillate around the theoretical solution during the first RT. For the third and the ninth waves, the oscillations become more and more chaotic (so-called spurious oscillations). Moreover, we observe a monotonic decrease of the slope of the wave fronts.

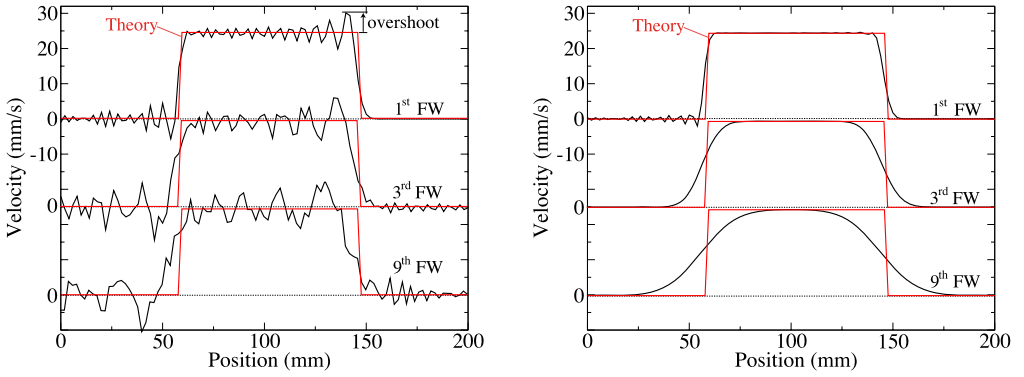

(a) Wave shape with the CD scheme (no damping)

(b) Wave shape with the TW scheme

Fig. 2. Wave shape along the 200 mm cylindrical rod. (For interpretation of the colours in this figure the reader is referred to the web version of this article.)

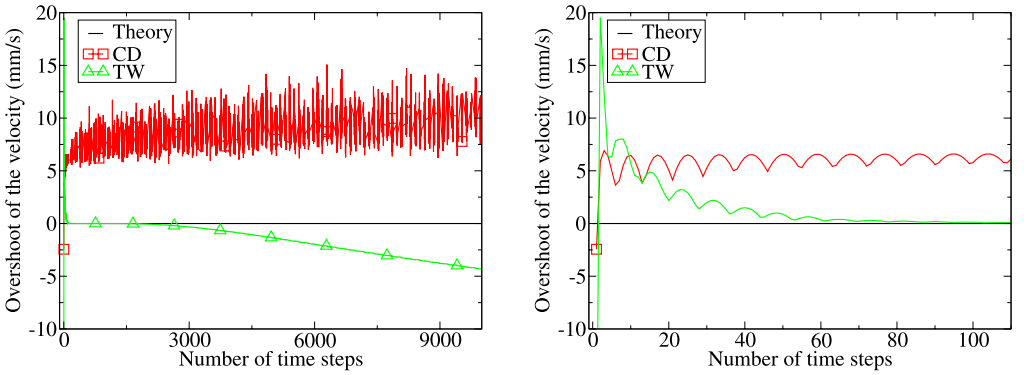

(a) 0 to 10 000Δt

(b) Zoom – 0 to 110Δt

Fig. 3. Overshoot of the velocity versus the number of the time step.

With the TW scheme (Fig. 2(b)), the spurious oscillations are quickly damped and the first forward wave is close to the theoretical solution. The sinusoidal black curves show that the square shape of the wave is progressively altered by the damping of the TW scheme.

We define the overshoot as the difference (absolute value) between the maximum velocity recorded within the rod and the theoretical velocity. The overshoot of the velocity is plotted in Fig. 3. In this figure, the overshoot is only plotted over an interval where the wave is free from any superimposition.

For the TW scheme, the damping efficiency can be observed in Fig. 3: the overshoot of the nodal velocities is completely damped after $60\Delta t$. After a propagation time of $2000\Delta t$, the damping of the nodal velocity becomes too strong and the maximum velocity does not reach the theoretical value. The value of the damping parameter $\varphi = 1.033$ appears to be too large in this case. However, $\varphi = 1.033$ is acceptable within the present framework of our study that focuses on the quick damping of spurious oscillations associated with instantaneous loadings. In Fig. 5(a), the corresponding remaining energy is shown as a function of the time step (green line with diamond marks, "100 el. (vs. Δt)" referenced). The apparent energy decrease is in line with the previous observations. Moreover, the energy is approximately independent of the reflections of the wave at the bar ends. In the following, the damping of the TW scheme is expressed in terms of the remaining energy.

In the case of the conservative CD scheme, the value of the overshoot is quickly increasing during the first $500\Delta t$. After this duration, the overshoot is still oscillating, but the mean value is slowly increasing from 8 mm/s to 12 mm/s. Furthermore, the energy remains constant during the whole calculation time when using the CD scheme.

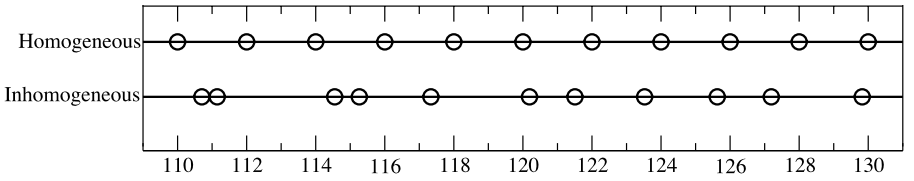

Fig. 4. Part of the homogeneous and inhomogeneous 1-D meshes.

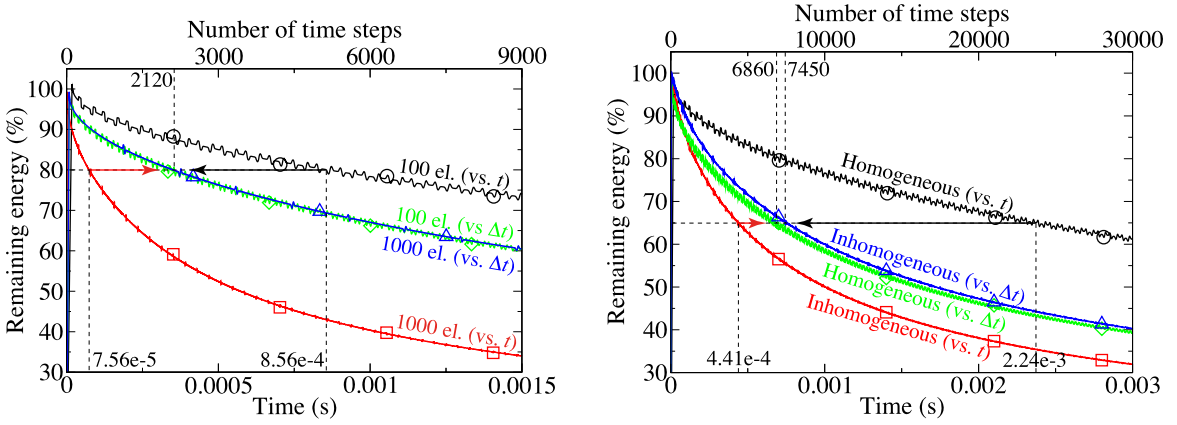

(a) Remaining energy with the homogeneous 1-D meshes

(b) Remaining energy with the inhomogeneous 1-D mesh

Fig. 5. Comparison between various 1-D meshes.

4.3. Influence of the meshing refinement

The damping obtained with each method was studied on two meshes composed of 100 and 1000 elements with a uniform length. In this case, the local critical time step Δt_c^i is equal to the global critical time step Δt_c and $r_{\Delta t}^i = r_{\Delta t}$. The remaining energy is presented in Fig. 5(a) with respect to time and the number of time steps. When plotted as a function of time, the damping achieved with the TW scheme can be clearly seen here to have depended on the number of elements used in the discretization procedure.

80% of the energy introduced into the system still remained after a propagation time of 7.56×10^{-5} s and 8.56×10^{-4} s with meshes consisting of 1000 and 100 elements, respectively. However, when these results were expressed in terms of the number of time steps, the damping turned out to be identical with both meshing configurations. 80% of the energy introduced into the system still remained after a propagation time of about $2120\Delta t$ with both meshes.

In the case of refined 1-D homogeneous meshes under instantaneous loading conditions, the damping efficiency depends on the number of times the TW dissipative scheme is applied.

4.4. Influence of the meshing irregularity

The damping efficiency of the TW scheme was assessed with an inhomogeneous 100-elements mesh. A random shift was applied to each node except for those at both ends. Nodal position was defined as follows:

$$x_{\text{new}} = x_{\text{old}} + \alpha_1 \frac{\bar{L}_e}{2}(1 - \alpha_2) \tag{9}$$

where x_{new} and x_{old} denote the new and previous nodal positions, respectively. $\alpha_1 \in [0, 1]$ defines the range of nodal positions. $\alpha_2 \in [0, 2]$ is a random number defining the position of a node in this range. Part of the two 200 mm-meshes is shown in Fig. 4. With the inhomogeneous mesh, the length of the smallest and the largest element is 0.33 mm and 3.81 mm, respectively. Since, the values of the critical time step of the homogeneous and inhomogeneous meshes are 3.91×10^{-7} s and 0.65×10^{-7} s, respectively.

The remaining energy is presented in Fig. 5(b) with respect to time and the number of time steps. 65% of the energy introduced into the system still remained after a propagation time of 2.24×10^{-3} s and 4.41×10^{-4} s with

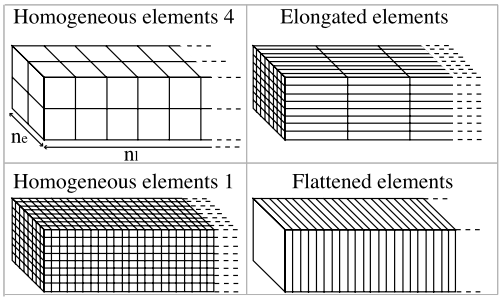

Fig. 6. Scale drawing of the homogeneous 3-D meshes.

the homogeneous mesh and the inhomogeneous mesh, respectively. However, when these results were expressed in terms of the number of time steps, the damping turned out to be quasi-identical with both meshes. 65% of the energy introduced into the system still remained after a propagation of $6860\Delta t$ and $7450\Delta t$ with the homogeneous mesh and the inhomogeneous mesh, respectively. The theoretical analysis in Section 3.1 shows that the damping can be related to the ratio $r_{\Delta t}$ by the expression $(\Delta t)^2\ddot{q}_n = -8(r_{\Delta t})^2 q_n$. In the case of inhomogeneous meshes, the local ratio $r^i_{\Delta t} \leqslant r_{\Delta t}$, which means that the damping efficiency decreased.

5. Three-dimensional damping efficiency under instantaneous loads

5.1. Description of the 3-D problem

Here we take the case of a square rod with a length of $L_{\text{rod}} = 200$ mm and a cross-sectional area of $S = 64$ mm^2, which is discretized into $n_e \times n_e$ elements across the section and n_l elements lengthwise. One end of the rod is fixed and an axial instantaneous compression load $P_0 = 10$ N with a square wave shape is applied to the free end:

- the pressure ramps P_0 at the beginning and $-P_0$ at the end of the square wave are simulated in $1\Delta t$,
- the plateau duration is equal to $48\Delta t$.

The elements used were fully integrated 8-node linear hexaedra with 8 integration points.

To prevent the size of time step from affecting the calculations [17], the same global ratio $r_{\Delta t} = \frac{\Delta t}{\Delta t_c}$ was used in all the calculations. In this section, the propagation involves a 3-D strain field. In order to study the influence of the meshing in the longitudinal and the transversal directions, let us take $r^L_{\Delta t} = \frac{\Delta t}{\Delta t^L_c}$ and $r^T_{\Delta t} = \frac{\Delta t}{\Delta t^T_c}$ to define the calculation time step – to critical time steps ratios in the longitudinal and the transversal directions, respectively.

5.2. Influence of the meshing refinement

The damping efficiency of the TW scheme was then studied using variously refined 3-D meshes. These meshes can be refined:

- lengthwise and the mesh is named *mesh with flattened elements*,
- across the section of the bar and the mesh is named *mesh with elongated elements*,
- both lengthwise and across the section of the bar and proportionally, in which case the meshes are named *meshes with homogeneous elements* 1 *and* 4.

The meshes used are presented in Fig. 6 and their characteristics are listed in Table 1.

For the sake of simplicity, the remaining energy is presented in Fig. 7(a) in terms of the number of time steps alone. Taking the mesh with homogeneous elements 1 as the reference mesh, the differences in the remaining energies are shown in Fig. 7(b).

In the meshes with *homogeneous elements* 1 *and* 4, the damping efficiency was found to be practically the same and the difference in remaining energy was about 1%. In this case, $r^L_{\Delta t} = r^T_{\Delta t} = r_{\Delta t}$ which shows that all these meshes have practically the same damping efficiency.

Table 1
Various 3-D meshes.

Meshes	Number of elements $n_e \times n_e \times n_l$
Homogeneous elements 4	$2 \times 2 \times 50$
Homogeneous elements 1	$8 \times 8 \times 200$
Elongated elements	$8 \times 8 \times 25$
Flattened elements	$1 \times 1 \times 200$
Homogeneous elements 2	$4 \times 4 \times 100$
Inhomogeneous elements 2	$4 \times 4 \times 100$

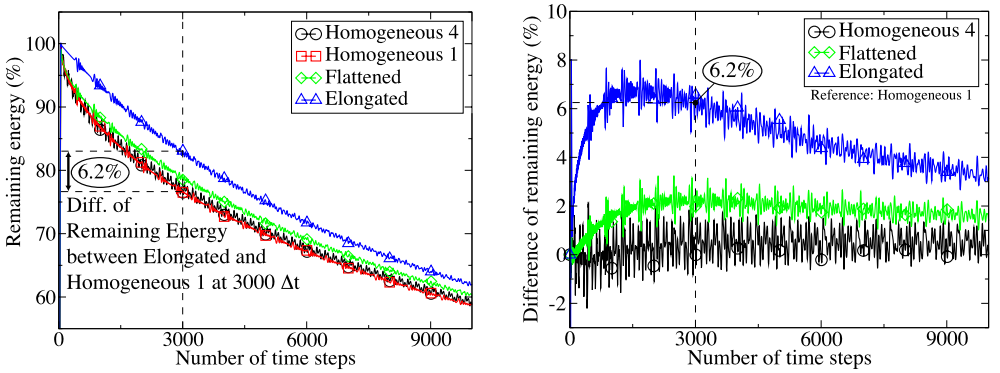

Fig. 7. Comparison between various homogeneous 3-D meshes. (a) Remaining energy with the 3-D meshes with homogeneous, flattened and elongated elements. (b) Difference in remaining energy, taking the mesh with homogeneous elements 1 as the reference mesh.

In the mesh with *flattened elements*, the damping is not so efficient at the beginning. A difference of 2% can be observed in Fig. 7(b) after a propagation of about $2000\Delta t$. In this case, $r^T_{\Delta t} < r_{\Delta t}$ and $r^L_{\Delta t} = r_{\Delta t}$. The axial instantaneous compression load results in a 3-D strain field due to the Poisson's effects, which leads to a dispersive propagation of the wave along the bar. The transversal component of the displacement is perturbed by the change in the meshing refinement, which decreases the damping efficiency, in line with the theoretical study presented in Section 3.1. However, this decrease is smaller than that occurring with the mesh with elongated elements because most of the energy propagates in the longitudinal direction. Other calculations were carried out using a null Poisson's ratio, i.e. without taking the dispersion into account, and applying a homogeneous velocity to the nodes at the free end. These conditions gave 1-D propagation and the damping efficiencies obtained with the meshes with flattened elements and homogeneous elements were identical. It is worth noting that the discretization procedure used in the propagation direction had considerable effects on the damping efficiency.

In the mesh with *elongated elements*, the damping efficiency decreased sharply at the beginning. A difference of 6.2% can be observed in Fig. 7(b) after a propagation time of about $3000\Delta t$. In this case, $r^L_{\Delta t} < r_{\Delta t}$ and $r^T_{\Delta t} = r_{\Delta t}$. The longitudinal component of the displacement is perturbed by the change in the meshing, which resulted in the largest decrease observed in the damping among all the meshes studied, in line with the theoretical study presented in Section 3.1. Similar results were obtained when a null Poisson's ratio was used in the calculations. This confirms the importance of the discretization procedure used in the propagation direction.

After a propagation time of $10\,000\Delta t$, the difference between the remaining energies decreased, reaching 1.5% and 3% in the meshes with flattened and elongated elements, respectively. The remaining energies and their differences subsequently tended towards zero.

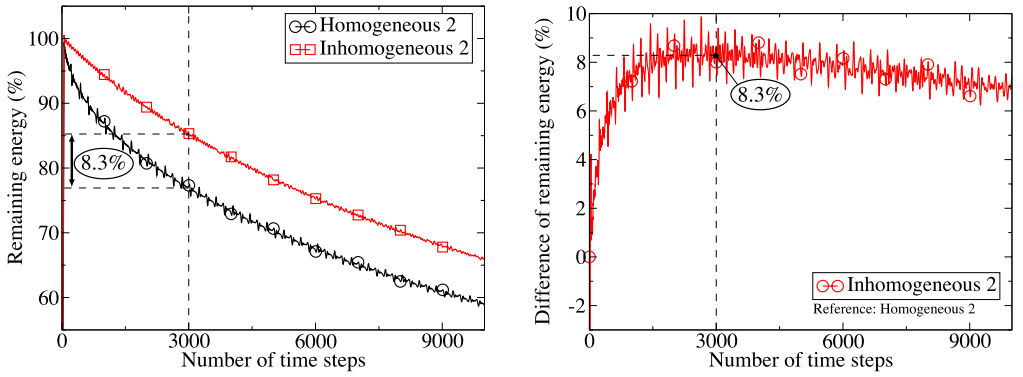

Fig. 8. Comparison between homogeneous and inhomogeneous 3-D meshes. (a) Remaining energy with the 3-D mesh with inhomogeneous elements. (b) Difference in the remaining energy taking the mesh with homogeneous elements 2 as the reference mesh.

5.3. Influence of the meshing irregularity

Lastly, the damping efficiency of the TW scheme was studied in the case of an inhomogeneous mesh in the lengthwise direction. Each section is discretized into $n_e \times n_e = 4 \times 4$ elements and the length of the bar was discretized into $n_l = 100$ elements. The same random shift as in Section 4.4 was applied lengthwise.

The remaining energy and the difference of remaining energy are presented with respect to the number of time steps in Figs. 8(a) and 8(b), respectively.

After a propagation time of $3000\Delta t$, a 8.3% difference in the remaining energy was observed between the mesh with homogeneous elements 2 and that with inhomogeneous elements 2. In this case, the transversal length was 2 mm and the smallest longitudinal length was 0.33 mm. Thus, $r^T_{\Delta t} < r_{\Delta t}$ and the damping efficiency of the transversal component of the displacement was perturbed by the change of the meshing. In addition, $r^i_{\Delta t} L \leqslant r_{\Delta t}$ with each element i and the damping efficiency of the longitudinal component of the displacement is also perturbed by the change of the meshing.

6. Conclusion

The explicit dissipative Tchamwa–Wielgosz scheme is known to be an efficient method of damping spurious oscillations. To complete previous research, a new theoretical study was performed and the influence of the meshing refinement and homogeneity on the damping efficiency was investigated under instantaneous loading conditions.

In the present theoretical study, it was established that the TW scheme was decentered to the right and its damping was attributed to a nodal displacement perturbation. The damping efficiency of the scheme was found to increase with the size of the time step – to critical time step ratio $r_{\Delta t} = \frac{\Delta t}{\Delta t_c}$.

In the numerical study presented above, various homogeneous and inhomogeneous 1-D and 3-D meshes were tested to determine the influence of the meshing configuration on the damping efficiency under instantaneous loading conditions. In order to be able to compare the various numerical examples, it was necessary to adopt the following two numerical conditions:

- To prevent the size of time step – to critical time step ratio $r_{\Delta t} = \frac{\Delta t}{\Delta t_c}$ from affecting the calculations and to obtain instantaneous loading conditions throughout, the same ratio was used in all the calculations.
- To make the results easier to interpret, the remaining energy was displayed versus the number of time steps.

In the case of the 1-D homogeneous meshes, the results showed that the damping efficiency depends on the number of times the dissipative TW scheme is applied. When plotted as a function of the number of calculation time steps, the damping efficiency was found to be independent of the size of the elements. In the case of the inhomogeneous 1-D meshes, with each element i, the local ratio $r^i_{\Delta t}$ is lower than the global ratio $r_{\Delta t}$, which confirmed that the damping

efficiency decreased. This is in line with the theoretical study, where the damping efficiency was found to be related to this ratio.

In the case of the homogeneous or inhomogeneous 3-D meshes, the results showed the importance of the discretization procedure used in the propagation direction. On similar lines, with each element i, the value of the calculation time step – to critical time step ratio in the longitudinal direction $r_{\Delta t}^{iL}$ and that of this in the transversal direction $r_{\Delta t}^{iT}$ were always lower than or equal to the value of the global ratio $r_{\Delta t}$, reflecting the decrease in the damping efficiency.

References

[1] J. Von Neuman, R.D. Richtmeyer, A method for numerical calculation of hydrodynamic shocks, J. Appl. Phys. 21 (1950) 232–237.

[2] R. Landshoff, A numerical method for treating fluid flow in the presence of shocks, Technical report, Los Alamos National Laboratory, 1955.

[3] ABAQUS Theory Manual, Version 6.7, Hibbitt, Karlsson & Sorensen, Inc., 2007.

[4] O. Hallquist, LS-Dyna 3D theoretical manual, Livermore Software Technology, 1998.

[5] H. Hilber, T. Hughes, R. Taylor, Improved numerical dissipation for time integration algorithms in structural dynamics, Earthquake Engineering Structural Dynamics 5 (1977) 283–292.

[6] W. Wood, M. Bossak, O.C. Zienkiewicz, An alpha modification of Newmark's method, Int. J. Numer. Meth. Eng. 15 (1981) 1562–1566.

[7] N.M. Newmark, A method of computation for structural dynamics, J. Eng. Mech. Div. ASCE (1959) 67–94.

[8] J. Chung, G.M. Hulbert, A time integration algorithm for structural dynamics with improved numerical dissipation: The generalized-α method, J. Appl. Mech. 60 (1993) 371–375.

[9] T.C. Fung, Numerical dissipation in time-step integration algorithms for structural dynamic analysis, Prog. Struct. Eng. Mater. 5 (2003) 167–180.

[10] J. Chung, J.M. Lee, A new family of explicit time integration methods for linear and non-linear structural dynamics, Int. J. Numer. Methods Eng. 37 (1994) 3961–3976.

[11] W.M. Zhai, Two simple fast integration methods for large-scale dynamic problems in engineering, Int. J. Numer. Methods Eng. 39 (1996) 4199–4214.

[12] G.M. Hulbert, J. Chung, Explicit time integration algorithms for structural dynamics with optimal numerical dissipation, Comput. Methods Appl. Mech. Eng. 137 (1996) 175–188.

[13] B. Tchamwa, Contributions à l'étude des méthodes d'intégration directe explicites en dynamique non linéaire des structures, PhD thesis, Ecole Centrale de Nantes, 1997 (in French).

[14] V. Grolleau, L. Mahéo, G. Rio, Numerical damping of spurious oscillations: A comparison between bulk-viscosity and dissipative explicit algorithms, in: A.A. Millpress (Ed.), Eurodyn 2005 Conference, Paris, Rotterdam, 2005.

[15] A. Soive, Apports à la méthode des éléments finis appliqués aux calculs de structures en dynamique rapide et amortissement numérique, PhD thesis, Université de Bretagne Sud, 2003 (in French).

[16] V. Grolleau, A. Soive, G. Rio, Une comparaison des schémas d'intégration temporelle explicites de Chung–Lee et Tchamwa–Wielgosz, C. R. Mécanique 332 (2004) 927–932.

[17] G. Rio, A. Soive, V. Grolleau, Comparative study of numerical explicit time integration algorithms, Adv. Eng. Softw. 36 (2005) 252–265.

[18] L. Mahéo, Etude des effets dissipatifs de différents schémas d'intégration temporelle en calcul dynamique par éléments finis, PhD thesis, Université de Bretagne Sud, 2006 (in French).

[19] N. Nsiampa, J.P. Ponthot, L. Noels, Comparative study of numerical explicit schemes for impact problem, Int. J. Impact Eng. 35 (2008) 1688–1694.

[20] G. Rio, Herezh++: FEM software for large transformations in solids, Dépôt APP (Agence pour la Protection des Programmes) – Certification IDDN.FR.010.0106078.000.R.P.2006.035.20600, Laboratoire d'Ingénierie des Matériaux de Bretagne, 2009.

[21] Laboratoire d'Ingénierie des MATériaux de Bretagne (Limatb), http://web.univ-ubs.fr/limatb, 2009.

[22] M. Géradin, D. Rixen, Mechanical Vibrations: Theory and Applications to Structural Dynamics, John Wiley & Son, Ltd., 1997.